



AFM-Based Manufacturing for Nano-fabrication Processes: Molecular Dynamics Simulation and AFM Experimental Verification

Rapeepan Promyoo^{1,*}, Hazim El-Mounayri¹ and Kody Varahramyan²

¹Department of Mechanical Engineering, Indiana University-Purdue University Indianapolis, Indiana, USA 46202

²Department of Electrical and Computer Engineering, Indiana University-Purdue University Indianapolis, Indiana, USA 46202

* Corresponding Author: Tel: 1 317 274 3091, Fax: 1 317 274 9744,

E-mail: rpromyoo@iupui.edu

Abstract

Recent developments in science and engineering have advanced the fabrication techniques for nanodevices, including the use of atomic force microscope (AFM) for nanomachining and nano-fabrication of nano-structures. AFM-based manufacturing generally involves nanoindentation and nanoscratching processes. This paper describes the development and validation of computational models for the AFM-based manufacturing for nano-fabrication processes. The Molecular Dynamics (MD) technique is used to model and simulate mechanical indentation at the nanoscale. MD simulation represents itself as a viable alternative to the expensive traditional experimental approach, which can be used to study the effects of various indentation variables including tool shape, indentation conditions, and material properties in a much more cost effective way. The simulation allows for prediction of the indentation forces at the interface between an indenter and a substrate. Also, the MD simulation is used to study the effects of speed on the indentation force. The material deformation and indentation geometry are extracted based on the final locations of atoms, which are displaced by the rigid indenter. In addition to modeling, an AFM was used to conduct actual indentation at the nanoscale, and provide measurements to validate the predictions from the MD simulation. It can be observed from the MD simulation results that the indentation force increases as the depth of indentation and tip radius increase, but decreases as the tip speed increases.

Keywords: Molecular Dynamics, MD Simulation, AFM-based Manufacturing, Nanoindentation.

1. Introduction

Recent developments in science and engineering have advanced the fabrication techniques for micro/nanodevices. Among them, AFM has been used for nanomachining and nanofabrication such as nanolithography, nano-writing, and nanopatterning [1-9]. AFM-based nanomachining generally involves nano-indentation and nanoscratching processes.

Nanoindentation and nanoscratching have been widely used to determine the mechanical properties of small-scale materials. Nano-channels, nanoslots, and complex nanopatterns can be fabricated by directly scratching the surface with an AFM [3]. For different applied loads, the depth and size of indents can be controlled. Nanoindentation can be used to fabricate cells for molecular electronics and drug



delivery, to make slots for the integration of nanowires into nanodevices, and to create defects on nanowires in order to change their structure and properties [4]. In addition, AFM nanoscratching in combination with a lift-off process can be used for the fabrication of metal nanowires [7-8]. Also, the application of nanoindentation and nanoscratching can be used in the field of ultraprecision machining [10]. Complex two- and three- dimensional micro/nano structures, such as line-type, concave and convex structures have been fabricated using AFM [11].

Typically, nanoindentation and nanoscratching have been experimentally conducted using AFM-based systems, which are complex and expensive. The phenomena that occur during nanoindentation and nanoscratching are atomic scale. Therefore, atomistic modeling is necessary to give insight into the underlying mechanisms and provide a fundamental understanding of both the process and its dependencies. Molecular dynamics (MD) simulation can be used to complement the traditional experiments. It has been successfully applied to investigate various phenomena at the nanoscale. The advantages of MD simulation over continuum models such as finite elements is that it allows a more complete and fundamental understanding of the way in which defects are created, the transition from elastic to plastic behavior, and crystal structure effects in materials [12]. Compared to the experimental approach, MD simulation does not require the use of expensive equipment but yet can be used to study the effects of various indentation variables including tool shape, indentation conditions, and material properties in a much more cost effective way.

Numerous studies have been reported on MD simulation of nanoindentation and nanoscratching [10,13-15]. However, MD simulation involves the interaction of a large number of atoms as deformation occurs on an atomic scale. One major concern in MD simulation is the high computational time required. In order to reduce it, many researchers developed two-dimensional models instead of the more realistic three-dimensional model. Two-dimensional based MD simulation is very computational efficient, but result in a significant loss of the quality of material representation. Another factor affecting the computational time is the number of atoms. The larger the number of atoms, the longer the computational time. To keep the processing time under control, most existing models of nanoindentation use less than 20,000 atoms. The largest models of nanoindentation found in the literature contain approximately 10 million atoms [16], which is enabled by parallel computing.

In this paper, three-dimensional MD simulations of nanoindentation in the case of gold, copper, aluminum and silicon are performed. The simulation allows for the prediction of indentation force at the interface between an indenter and a substrate. The effects of tip speed and tip radius on indentation force are investigated. The material deformation and indentation geometry are extracted based on the final locations of the atoms, which have been displaced by the rigid tool. In addition, an AFM system is used to conduct actual indentation at the nanoscale, and provide data to validate the MD simulation. The results of the simulation as well as the AFM data are presented and compared.

2. Methodology

MD simulation is used to simulate the time dependent behavior of a molecular system. The inputs required in MD simulation are initial positions and velocities of atoms in the system along with other information such as boundary conditions, potential energy function, time steps, etc. The outputs of the simulation include trajectories of atoms in the system, forces, energy of the system, and other physical quantities of interest. The MD simulation model and the potential functions used in this study are explained in the following sections.

2.1 Simulation Model

The schematic model used in the MD simulation of nanoindentation is shown in Fig. 1. The initial positions of atoms in the model are calculated from the default lattice position. In this study, single crystal gold (Au), copper (Cu), aluminum (Al) and silicon (Si) are chosen as workpiece materials and diamond is selected as an indenter. The diamond indenter is considered as a rigid body. The simulation model consists of a single crystal workpiece and a three-sided pyramidal indenter. The workpiece in the MD simulation is divided into three different zones: the boundary zone, the thermostat zone, and the Newtonian zone.

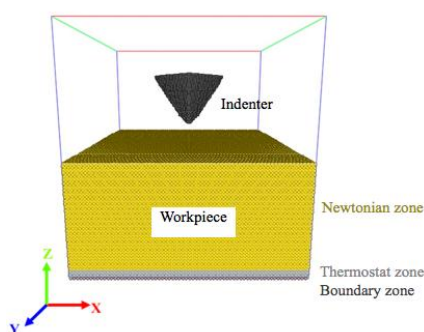


Fig. 1 Schematic MD simulation model of nanoindentation

Two layers of boundary atoms and six layers of thermostat atoms are placed on the bottom side of the workpiece. Fixed boundary conditions are applied to the boundary atoms. The atoms are fixed in the position to reduce the edge effects and maintain the symmetry of the lattice. Periodic boundary conditions are maintained along the x- and y-direction. The periodic boundary conditions are usually employed when a simulation seek to investigate the behavior of an isolated system, to avoid spurious edge effects, and thereby simulate the behavior of a much larger crystal system. The thermostat zone is included in the MD simulation model to ensure that the heat generated during the indentation process can be conducted out of the indentation region properly. The temperature in the thermostat zone is maintained by scaling the velocities of the thermostat atoms for each computational time step. In the Newtonian zone, atoms move according to Newton's equation of motion.

2.2 Potential Energy Function

The motion of the atoms in the Newtonian zone is determined by the forces derived from potential energy function and Newton's equation of motion. The interaction of each atom can be approximated by a potential energy function in accordance with Newtonian mechanics. The quality of the MD simulation results depends on the accuracy of the potential energy function used. On the other hand, the complexity of the potential energy function directly affects the computational time [17]. The selection of the potential function depends on the type of material used in the model. For the case of gold,

copper and aluminum atoms, potential energy functions used are the Morse potential [18] and the Embedded-atom method (EAM) potential [19]. The EAM potential is employed for the interaction between atoms in the workpiece material for gold, copper and aluminum. The Morse potential is employed for the interaction between atoms in the workpiece and carbon atoms in the diamond tip in the MD simulations (Au-C, Cu-C and Al-C). For the case of silicon, Tersoff potential [20] will be employed for both interactions between silicon atoms in the workpiece material (Si-Si) and between silicon and carbon (Si-C) atoms.

The interatomic force between any two atoms can be obtained from the potential energy function as shown in Eq. 1, where F_{ij} is the interatomic force between atom i and j at a distance r_{ij} from atom i .

$$F_{ij} = -\frac{\partial U}{\partial r_{ij}} \quad (1)$$

The total force exerted on a particular atom is then calculated based on Eq. 2, where F_i is the resultant force on atom i and N is the total number of atoms.

$$F_i = \sum_{j=1, i \neq j}^N F_{ij}(r_{ij}) \quad (2)$$

After calculating force on each atom, velocities and positions are calculated from Newton's second law of motion.

2.4 MD Simulation Conditions

MD simulation of nanoindentation was conducted on single crystal gold, copper, aluminum and silicon. Parallel MD simulations were implemented using LAMMPS [21-22]. Simulation was conducted along the (001) direction of crystal. Table. 1 gives the conditions

used in the MD simulation. The dimensions of the workpiece and indenter, the depth of indentation and the tip speed are given. The dimensions of the workpiece are expressed in terms of lattice constants. The lattice constants of gold (a_{Au}), copper (a_{Cu}) and aluminum (a_{Al}) are 4.080, 3.615, and 3.986 Angstroms (Å), respectively, while the lattice constant of silicon (a_{Si}) is 5.431 Å.

3. Experimental Setup

Table. 1 MD simulation conditions used in the MD simulations of nanoindentation

Workpiece material	Gold (Au), Copper (Cu), Aluminum (Al), Silicon (Si)
Workpiece dimension	Au: $150a_{Au} \times 150a_{Au} \times 70a_{Au}$, $150a_{Au} \times 150a_{Au} \times 150a_{Au}$ Cu: $150a_{Cu} \times 150a_{Cu} \times 70a_{Cu}$ Al: $150a_{Al} \times 150a_{Al} \times 70a_{Al}$ Si: $100a_{Si} \times 100a_{Si} \times 50a_{Si}$
Number of atoms in the workpiece	Au: 6,300,000 atoms 13,500,000 atoms Cu: 6,300,000 atoms Al: 6,300,000 atoms Si: 4,000,000 atoms
Indenter tip material	Diamond
Indenter type	Three sided pyramid
Tip apex angle	60°
Tip radius	0, 25, 50, 75, 100 nm
Indentation depth	5 - 60 nm
Nanoindentation tip speed	0.1, 1, 10 m/s
Bulk temperature	293 K
Time steps	1 fs (10^{-15} s)

A Veeco Bioscope AFM was used to conduct actual indentation at the nanoscale, and

provide data for evaluating the MD simulation predictions. The AFM provides resolution on the nanometer (lateral) and angstrom (vertical) scales. A three-sided pyramid indenter with a radius of curvature ~ 50 nm was used in the experiments. The diamond tip has an apex angle of about 60 degrees. Here, the apex angle is the angle between a face and an edge on the opposite side of the tip.

Nanoindentation experiments were conducted on $8 \times 8 \times 2$ mm³ gold sample. The nanoindentation experiments were conducted at indentation depths of 20, 30, and 40 nm. The tip speed used was 10 μ m/s.

4. Results and Discussion

4.1 MD Simulation of Nanoindentation

MD simulation snapshots of nano-indentation for the cases of gold at various times are shown in Figs 2(a) -2(f). The figures show the initial stage of indenter tip and workpiece material in nanoindentation followed by the movement of the tip into the workpiece material at various time intervals. The workpiece atoms are compressed beneath the tip and the deformation in workpiece material can be seen in the vicinity of the tip. The material apart from the tip seems to be very slightly affected by the motion of the tip. After the tip is moved away from the surface, some of the workpiece atoms are deposited onto the surface of the diamond indenter. All MD simulation snapshots are visualized by Atomeye [23].

Surrounding the contact surface between the indenter and the workpiece, a material pile-up is observed. Figs. Top and cross-sectional views of MD simulation snapshots of nanoindentation for the case of gold are shown in Figs. 3 – 4,

respectively. Figs. 3(a) and 4(a) show the initial stage of nanoindentation, before the indenter comes into contact with the surface of workpiece material. At this stage, no deformation can be observed. Figs. 3(b) - 3(f) and 4(b) – 4(f) show the top and cross-sectional views of MD simulation snapshots of nanoindentation with the use of five different indenter tip radius (r), including 0, 25, 50, 75, and 100 nm, at the indentation depth of 10 nm. More surface deformation can be observed with the increasing indenter tip radius.

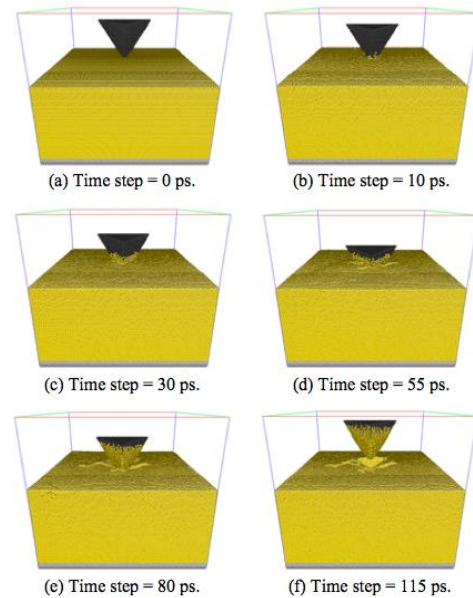


Fig. 2 MD simulation snapshots of nano-indentation of gold at various times: (a) 0 ps; (b) 10 ps; (c) 30 ps; (d) 55 ps; (e) 80 ps; (f) 115 ps

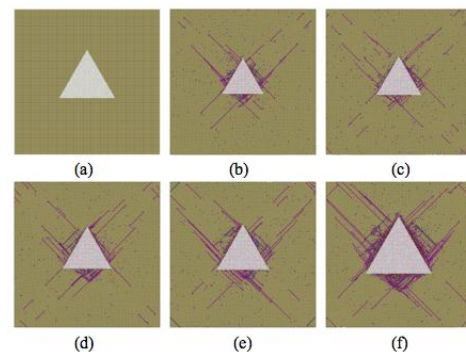


Fig. 3 Top views of MD simulation snapshots of nanoindentation of gold with the use of different

indenter tip radius (r): (a) initial stage of nanoindentation; (b) $r = 0$ nm; (c) $r = 25$ nm; (d) $r = 50$ nm; (e) $r = 75$ nm; (f) $r = 100$ nm.

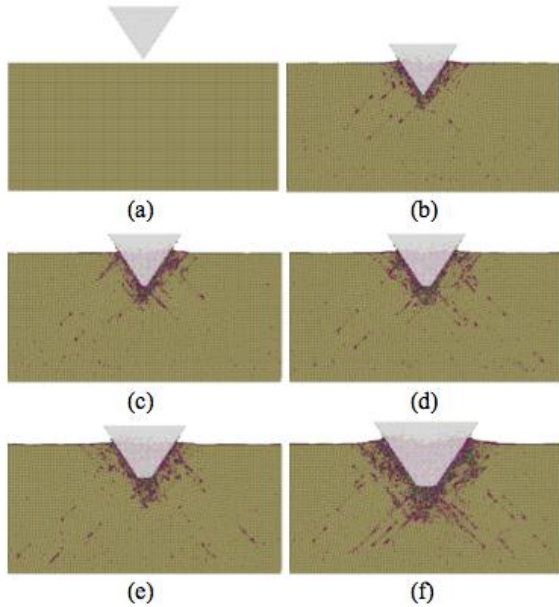


Fig. 4 Cross-sectional views of MD simulation snapshots of nanoindentation of gold with the use of different indenter tip radius (r): (a) initial stage of nanoindentation; (b) $r = 0$ nm; (c) $r = 25$ nm; (d) $r = 50$ nm; (e) $r = 75$ nm; (f) $r = 100$ nm.

The different colors shown in Figs. 3 – 4 represent coordination number, which is a measure of how many nearest neighbors exist for a particular atom. The purpose of using this coordination number coloring is to clearly see the defects and dislocations of atoms. It can be seen from Fig. 4 that as the tip radius increases, more subsurface deformation can be observed and the deformation is found to penetrate much deeper from the surface.

Figs. 5(a) - 5(b) show the top and cross-sectional views of MD simulation snapshots of the nanoindentation of gold. Fig. 6(a) – 6(b) show AFM images of the nanoindentation mark and indentation profile for the case of gold from a nanoindentation experiment with an indentation

depth of 30 nm. Material pile-up around the indentation marks can be observed for both simulation (Fig. 5) and experimental results (Fig. 6).

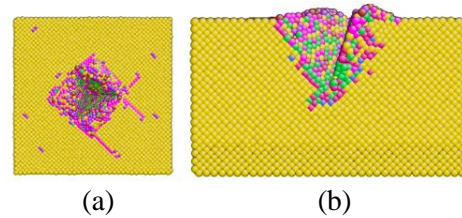


Fig. 5 Top (a) and cross-sectional (b) views of MD simulation snapshots of nanoindentation of gold.

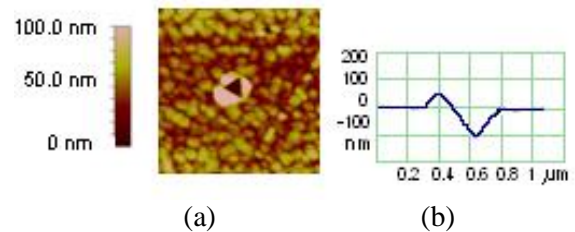


Fig. 6 Experimental results of nanoindentation of gold with an indentation depth of 30 nm: (a) AFM image of indentation mark (b) cross-sectional profile

Figs. 7 - 8 show, respectively, top and cross-sectional views of MD simulation snapshots of nanoindentation of different types of material: (a) gold; (b) copper; (c) silicon and (d) aluminum. The surface deformation can be observed in Fig. 7, while the subsurface deformation can be seen in Fig. 8. Gold, copper and aluminum have the same type of crystal structure, which is face-centered cubic (fcc) structure, while silicon has diamond structure. The surface and subsurface deformation found in the case of gold, copper and aluminum have the same pattern. However, it can be seen that aluminum has more surface deformation than other materials. For the case of silicon, the deformation can be observed only in the region surrounding the indenter tip. The

silicon atoms below the indentation mark become amorphous. In addition, there is no material pile-up at the surrounding of the contact surface between the indenter and the silicon workpiece.

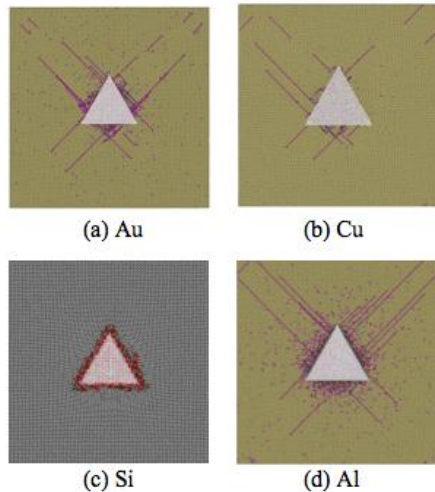


Fig. 7 Top views of MD simulation snapshots of nanoindentation of different materials: (a) gold; (b) copper; (c) silicon; (d) aluminum.

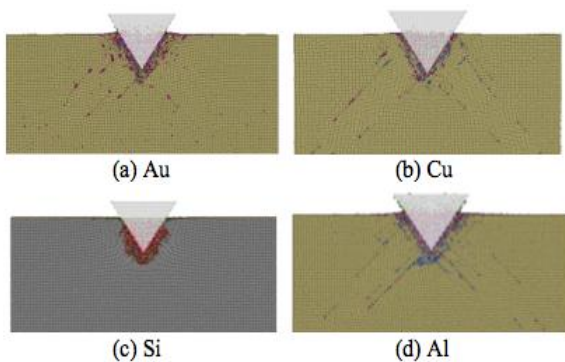


Fig. 8 Cross-sectional views of MD simulation snapshots of nanoindentation of different materials: (a) gold; (b) copper; (c) silicon; (d) aluminum.

4.2 Indentation Force

The variation of indentation forces with depths of indentation at different tip speeds is shown in Fig. 9. It can be observed that the indentation force increases with indentation depth. The simulation results were compared with their experimental counterparts. Due to limitations in

computational time, it should be noted that the tip speeds used in this MD simulation are a lot higher than those used in the experiment. The typical speed used in the experiment was approximately 5-10 $\mu\text{m/s}$, whereas the speed used in the MD simulation was 0.1-10 m/s. Therefore, the effect of tool tip speed on the indentation force is also investigated in this paper. It can be observed from Fig. 9 that the indentation force increases with tool tip speed. Since the tip speed plays an important role in the level of indentation force, the quantitative values of the latter obtained from MD simulation are not comparable to the experimental results. However, the trends are the same for both simulation and experimental results.

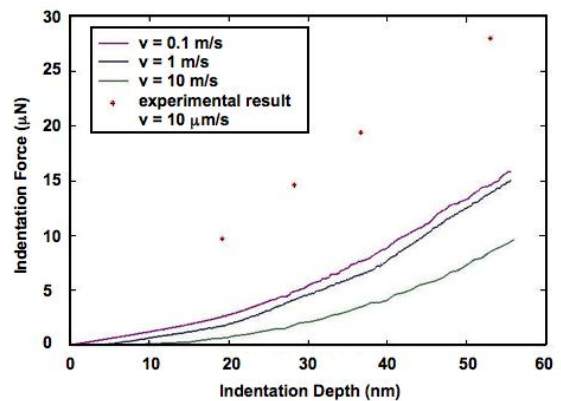


Fig. 9 Variation in indentation forces with depths of indentation at different tip speeds

Fig. 10 shows the variation in indentation forces with time step at different tool tip radius. It can be found that the indentation force increases with the increasing tip radius.

6. Conclusion

MD simulation of nanoindentation was conducted and validated by qualitative comparison with experimental measurements. The indentation forces at various depths of indentation were obtained. It can be concluded

that indentation force increases with depth. The effect of tool tip speed on the indentation force was also investigated and the force was found to be dependent on the tip speed. Moreover, the effect of tip radius on the indentation force was studied and can be concluded that the indentation force increases as the tip radius increases.

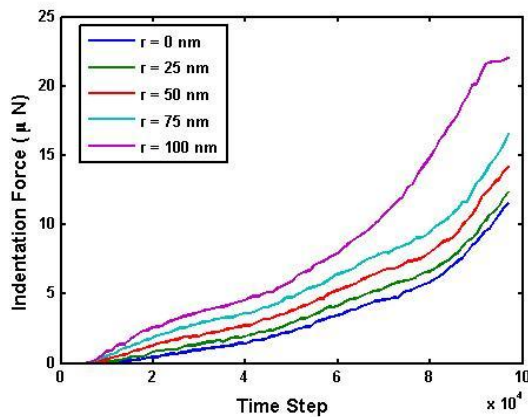


Fig. 10 Variation in indentation forces with time step at different tip radius.

7. References

- [1] Fischer-Cripps, A.C. (2002). *Nanoindentation*, Springer, New York.
- [2] Nie, X., Zhang, P., Weiner, A.M. and Cheng, Y.T., (2005). Nanoscale wear and machining behavior of nanolayer interfaces, *Nano Letters*, Vol. 5, pp. 1993-1996.
- [3] Li, X., Nardi, P., Baek, C.W., Kim, J.M. and Kim, Y.K., (2005). Direct nanomechanical machining of gold nanowires using a nanoindenter and an atomic force microscope, *Journal of Micromechanics and Microengineering*, Vol. 15, pp. 551-556.
- [4] Li, X., Gao, H., Murphy, C.J. and Caswell, K.K., (2003). Nanoindentation of silver nanowires, *Nano Letters*, Vol. 3, pp.1495-1498.
- [5] Yan, Y.D., Sun, T., Zhao, X.S., Hu, Z.J. and Dong, S., (2008). Fabrication of microstructures on the surface of a micro/hollow target ball by AFM, *Journal of Micromechanics and Microengineering*, Vol. 18, 035002.
- [6] Fang, T, Weng, C. and Chang, J., (2000). Machining characterization of the nanolithography process using atomic force microscopy, *Nanotechnology*, Vol. 11, pp. 181-187.
- [7] Chen, Y.J., Hsu, J.H. and Lin, H.N., (2005). Fabrication of metal nanowires by atomic force microscopy nanoscratching and lift-off process, *Nanotechnology*, Vol. 16, pp. 1112-1115.
- [8] Hsu, J.H., Huang, M.H., Lin, H.H. and Lin, H.N., (2006). Selective growth of silica nanowires on nickel nanostructures created by atomic force microscopy nanomachining, *Nanotechnology*, Vol. 17, pp. 170-173.
- [9] Ahn, B. W. and Lee, S. H., (2009). Characterization and acoustic emission monitoring of AFM nanomachining, *Journal of Micromechanics and Microengineering*, Vol. 19, 045028.
- [10] Komanduri, R., Chandrasekaran, N. and Raff, L.M., (2000). MD simulation of indentation and scratching of single crystal aluminum, *Wear*, Vol. 240, pp. 113-143.
- [11] Yan, Y., Sun, T., Liang, Y., and Dong, S., (2007). Investigation on AFM-based micro/nano-CNC machining system, *International Journal of Machine Tools and Manufacture*, Vol. 47, pp. 1651-1659.
- [12] Cheong, W.C.D. and Zhang, L.C., (2000). Molecular dynamics simulation of phase transformations in silicon monocrystals due to nano-indentation, *Nanotechnology*, Vol. 11, pp. 173-180.
- [13] Gheewala, I., Smith R. and Kenny, S.D., (2008). Nanoindentation and nanoscratching of



rutile and anatase TiO₂ studied using molecular dynamics simulations, *Journal of Physics: Condensed Matter*, Vol. 20, 354010.

[14] Liang, Y., Chen, J., Chen, M., Song, D. and Bai, Q., (2009). Three-dimensional molecular dynamics simulation of nanostructure for reciprocating nanomachining process, *Journal of Vacuum Science and Technology B*, Vol. 27, pp. 1536-1542.

[15] Gao, Y., Lu, C., Huynh, N.N., Michal, G., Zhu, H.T. and Tieu, A.K., (2009). Molecular dynamics simulation of effect of indenter shape on nanoscratch of Ni, *Wear*, Vol. 267, pp. 1998-2002.

[16] Komanduri, R., and Raff, L.M., (2001). A review on the molecular dynamics simulation of machining at the atomic scale, *Proceedings Institution of Mechanical Engineers*, Vol. 215, Part B, pp. 1639-1672.

[17] Walsh, P., Kalia, R.K., Nakano, A. and Vashishta, P., (2000). Amorphization and anisotropic fracture dynamics during nanoindentation of silicon nitride: A multimillion atom molecular dynamics study, *Applied Physics Letters*, Vol.77, pp.4332-4334.

[18] Morse, P.M., (1929). Diatomic molecules according to the wave mechanics II vibrational levels, *Physical Review*, Vol. 34, pp. 57-64.

[19] Daw, M.S. and Baskes, M.I., (1984). Embedded-atom method: Derivation and application to impurities, surfaces, and other defects in metals, *Physical Review B*, Vol. 29, pp. 6443-6453.

[20] Tersoff, J., (1988). New empirical approach for the structure and energy of covalent systems, *Physical Review B*, Vol. 37, pp. 6691-7000.

[21] Plimpton, S. J., (1995). Fast parallel algorithms for short-range molecular dynamics, *Journal of Computational Physics*, Vol. 117, pp. 1-19.

[22] Plimpton, S. J., Pollock, R., and Stevens, M., (1997). Particle-mesh Ewald and rRESPA for parallel molecular dynamics simulations, *Proc of the Eighth SIAM Conference on Parallel Processing for Scientific Computing*, Minneapolis, MN.

[23] Li, J., (2003). AtomEye: an efficient atomistic configuration viewer, *Modeling and Simulation in Materials Science and Engineering*, Vol. 11, pp. 173-177.